



# Non-isothermal crystallization kinetics of polypropylene/polytetrafluoroethylene fibrillated composites

Yuhui Qiao<sup>1,2,3</sup>, Amirjalal Jalali<sup>3</sup>, Jinian Yang<sup>3,4</sup>, Yuguang Chen<sup>3</sup>, Shiwei Wang<sup>1,2</sup>, Yongchao Jiang<sup>2</sup>, Jianhua Hou<sup>1,2</sup>, Jing Jiang<sup>2</sup>, Qian Li<sup>1,2,\*</sup>, and Chul B. Park<sup>3,\*</sup>

<sup>1</sup>School of Mechanics and Safety Engineering, Zhengzhou University, Zhengzhou 450001, People's Republic of China

<sup>2</sup>National Center for International Research of Micro-Nano Molding Technology, Zhengzhou University, Zhengzhou 450001, People's Republic of China

<sup>3</sup>Microcellular Plastics Manufacturing Laboratory, Department of Mechanical and Industrial Engineering, University of Toronto, Toronto M5S 3G8, Canada

<sup>4</sup>School of Materials and Engineering, Anhui University of Science and Technology, Huainan 232001, People's Republic of China

Received: 27 May 2020

Accepted: 3 September 2020

Published online:  
26 October 2020

© Springer Science+Business  
Media, LLC, part of Springer  
Nature 2020

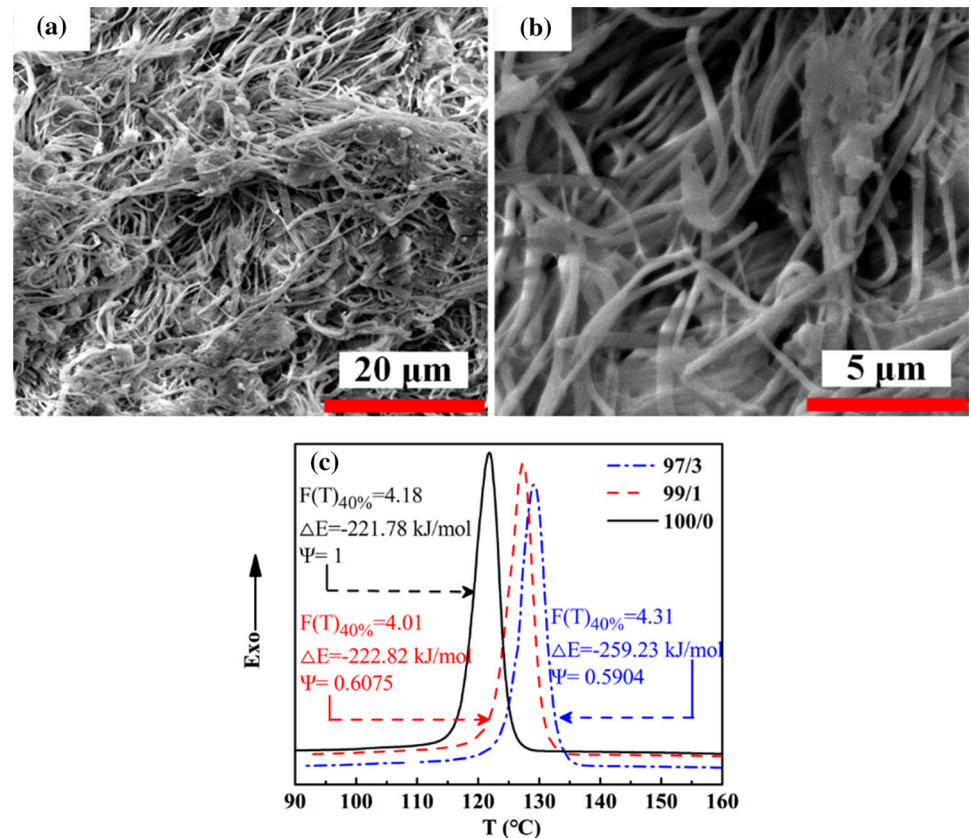
## ABSTRACT

Non-isothermal crystallization kinetics of polypropylene (PP)/polytetrafluoroethylene (PTFE) fibrillated composites is presented. In-situ fibrillated PP/PTFE-composites containing 1 and 3 wt% PTFE were prepared by melt compounding using a twin-screw extruder. The morphology and non-isothermal crystallization behavior of the composites were examined using scanning electron microscopy and differential scanning calorimetry, respectively. The Mo equation was used to analyze the kinetics of non-isothermal crystallization behavior. The PTFE created a three-dimensional (3-D) network. A low PTFE content promoted crystallization through fast nucleation, whereas a high PTFE content decreased the crystallization kinetics through hindering the crystal growth. These findings are all based on the Mo equation analysis. The activation energy and nucleation activity were also evaluated, and the way in which the PTFE nanofibers affected the crystallization was discussed in detail. Polarized optical microscopy images revealed that the size of PP spherulites decreased with the increase of PTFE content. Finally, the effect of PTFE on the crystalline phase of PP was investigated by wide angle X-ray diffraction.

Handling Editor: Gregory Rutledge.

Address correspondence to E-mail: qianli@zzu.edu.cn; park@mie.utoronto.ca

## GRAPHIC ABSTRACT



## Introduction

As a very widely used thermoplastic resin, polypropylene (PP) is widely used in packaging, appliances, automotive materials, industrial and household goods. In these areas, it serves as films, sheets, tubes, blocks, and so on. However, its low melt strength and lack of strain hardening in extensional flow largely limit its applications in foaming and film blowing [1–4]. Therefore, many efforts have been made to improve PP's melt strength to broaden its applications. Of these, Blending PP with other polymers, has been developed and has been increasingly used to design novel materials. For blends, successful interactions between the dispersed phase and the continuous matrix play a great role in improving the PP blends' melt strength. Many factors

affect the interactions between the matrix and the dispersed phase, and the configuration of the second phase is, especially crucial. A dispersed polymer with spherical droplets usually demonstrates weak interactions with the PP matrix; however, by creating a 3D network structure, the interaction could be strengthened.

Over the past decade, polytetrafluoroethylene (PTFE) has been considered as one of the most important modifiers in PP blends. It is well-known that PTFE particles transform to elongated fibers by high shear and extensional forces during processing [5–12]. Van der Meer et al. [13] blended PTFE particles of different sizes with PP. The larger PTFE (the average particle diameter was 600 μm) particles were deformed into fibrils and visible fibrillation could not be seen for the smaller particles with an average diameter of around 7 μm. Jurczuk et al. [6] found that

the generation of fine PTFE fibrils during the processing of PTFE particles dispersed in a molten polymer not only needs longer and stronger shear stress, but also has requirements to PTFE particles, such as high crystallinity and crystals with the high melting point. The entangled PTFE fibrils create a 3-D network in the matrix and such a network is preferred during foaming because it induces strain hardening and improves the melt strength [9, 14, 15], which are both crucial for enhancing foaming ability. Rizvi et al. [7, 16] showed that PP/PTFE fibrillated composites had up to three orders of magnitude higher cell number density and a ten-fold increase in the volume expansion ratio [7]. Jurczuk et al. [17] found that PTFE nanofibers resulted in smaller cell size and a higher cell density in extrusion foaming. Similar results in injection foaming were also obtained by Zhao et al. [18].

The effects of PP crystallization on foaming should not be overlooked [19, 20]. These include supersaturation, the application of tensile stress to the polymer melt by shrinkage, and the generation of local tensile stresses. Each of these processes contributes to cellular nucleation. The presence of PP crystals also helps to achieve a relatively high expansion ratio during foaming. This is due to the enhanced melt strength that results at a high foaming temperature [21]. The ability of PTFE to fibrillate is always used to nucleate PP crystallization. Wittmann and Smith [22] employed friction-deposited PTFE as substrate to induce oriented growth of several polymers, such as poly(Ethylene terephthalate), polyethylene, nylon 6, and nylon 11. A similar method is used by Yan et al. [23] and the results showed isotactic polypropylene in its  $\alpha$  modification crystallized epitaxially on PTFE via (110) plane. Frey et al. [24] prepared highly oriented polysilylene films by the method of Wittmann and Smith [22]. Transcrystallization of PP on PTFE fiber has also been studied. Using optical microscopy, Wang et al. [25, 26] demonstrated that PP crystallization probably occurred on PTFE fibers rather than in the bulk, because PTFE has lower interfacial free energy difference function ( $\Delta\sigma$ ) compared to that of the bulk. It has also been reported that the growth of a transcrystalline layer was impeded by the spherulites nucleated in the bulk. The radius of spherulites adjoining the transcrystalline layer was significantly smaller than that far away from the fiber. Considering that polymer solidification follows during non-isothermal conditions in practical processing, a

detailed examination of non-isothermal crystallization also seems to be important. Until now, however, the non-isothermal crystallization of fibrillated PP/PTFE-composites has not been widely studied in the literature [10, 17, 27], and rare reports have focused on the non-isothermal crystallization kinetics analysis.

In this study, fibrillated composites of PP/PTFE were prepared using a twin-screw extruder and the morphology of the fabricated composite was investigated. In addition, crystallization kinetics under non-isothermal conditions was studied using different theoretical models. The apparent activation energy and the nucleation activity for the composites were evaluated from the non-isothermal curves obtained by differential scanning calorimetry (DSC). Moreover, in order to assess the effect of PTFE fibers on PP crystallization morphology, polarized optical microscopy (POM) was used. Finally, the effect of fibrillated PTFE on the crystalline structure of PP was studied by X-ray diffraction.

## Materials and methods

### Materials

The polypropylene (PP, homopolymer, H521, granules,  $\overline{M}_n = 1.16 \times 10^5$  g/mol, the molecular weight distribution is 4.25) used in this study was supplied by the Braskem Co., Ltd (USA). Its melt flow rate (MFR) was 3.6 g/10 min (230 °C and 2.16 kg). The melting point of PP is 165 °C. The powdered PTFE (Metablen<sup>TM</sup> A-3000, powder) was supplied by the Mitsubishi Rayon Company (Japan). Its melting point is 345 °C. The PTFE particles tended to agglomerate into small clusters with around 8  $\mu\text{m}$  [28].

### Sample preparation

Prior to mixing, PP and PTFE were dried separately at 65 °C for at least 12 h under vacuum. The composites with a mass ratio of PTFE varying from 0 wt% to 3 wt%, and marked as 100/0, 99/1, and 97/3, respectively, were melt-compounded using a Leistritz co-rotating twin-screw extruder under the open air. The screw diameter was 27 mm and the L/D ratio was 40. The temperature profile was 120, 150, 190, 190, 190, 190, 190, 190, 185 and 180 °C from the hopper to the die. A high screw speed of 250 rpm,

which was much higher than the reported values [6, 29], was chosen for these experiments. Screw configuration (Figure S1) has been optimized based on the previous study of the laboratory.

## Characterization

### *Morphological observation*

The pellets of PP/PTFE nanofibril composites were compressed into a 500  $\mu\text{m}$  thick film at 190  $^{\circ}\text{C}$  and 10 MPa. The film was cut into  $1 \times 1$  cm squares, which were wrapped in the steel mesh and then put into a round-bottomed flask with xylene. The flask was immersed in an oil bath to heat the xylene to 140  $^{\circ}\text{C}$ . After 1 h, the PP in the PP/PTFE nanofibril composites was completely dissolved and the disks were taken out and cleaned in an ultrasonic bath. Then, the morphological structure of the PTFE fibrils obtained was examined. A scanning electron microscope (SEM, JEOL 6060, JEOL Ltd. Japan) was used to observe the sample morphology and to obtain digital images. Before the examination, the nonconductive samples were sputter-coated with a thin layer of platinum.

### *Differential scanning calorimetry (DSC)*

The crystallization measurements were made using DSC (Q2000, TA Instruments, USA). The weight of the samples was kept between 8.0 and 10.0 mg. To obtain the non-isothermal behavior, the samples were heated to 210  $^{\circ}\text{C}$ , held for 5 min, and then cooled to room temperature. The thermograms were recorded at cooling rates of 5, 10, 15, and 20  $^{\circ}\text{C}/\text{min}$ . In order to calculate the crystallinity, the samples were heated to 200  $^{\circ}\text{C}$  at 10  $^{\circ}\text{C}/\text{min}$ . All of the tests were performed under a  $\text{N}_2$  atmosphere (50 mL/min).

### *Polarized optical microscopy (POM)*

The effect of PTFE fibrils on the crystallization behavior of PP was investigated using POM (Olympus BX51, Japan) with a Linkam LTS 420E hot stage. Samples were pelletized, remelted, squeezed between glass slides at 200  $^{\circ}\text{C}$  for 5 min, and then rapidly cooled to 140  $^{\circ}\text{C}$ . The samples were isothermally crystallized at 140  $^{\circ}\text{C}$  until crystals touched each other.

### *Wide-angle X-ray diffraction (WAXD)*

The crystalline structure of PP in the samples was studied using WAXD. The X-ray diffraction patterns were collected at room temperature (25  $^{\circ}\text{C}$ ) with a Bruker D8 Advance diffractometer using germanium monochromatic radiation ( $\text{CuK}\alpha$ ). The data in the 2 $\theta$  range 5–35 $^{\circ}$  were collected in steps of 0.02 $^{\circ}$  with a holding time of 1 s per step under tube conditions of 40 kV and 10 mA. XRD traces were obtained for PP and PP/PTFE nanofibril composites isothermally crystallized at 140  $^{\circ}\text{C}$  for 40 min.

## Results and discussion

### Morphology

The phase morphologies of PP and PP/PTFE nanofibril composites are shown in Fig. 1. The neat PP (Fig. 1a) showed a clear flat surface, while the PP/PTFE nanofibril composites (Fig. 1b and c) clearly showed two phases, indicating immiscibility between PP and PTFE [12, 26]. Moreover, the composites exhibited a sea-island phase structure, and PTFE existed in the form of fiber. In order to observe stretched PTFE fibrils, selective etching was carried out. Figure 2 shows the morphological structure of the PP/PTFE (97/3) nanofibril composites etched in hot xylene. Due to the PP phase's dissolution, PTFE was clearly observable by the SEM. The PTFE phase exhibited a spatial distribution network consisting of fine PTFE nanofibrils. The average diameter of the fibrils was 245 nm, while the junctional particle could be seen and the sizes ranged broadly from 1 to 3  $\mu\text{m}$ . This outcome was very different from the results reported by other researchers [6, 7, 10, 12, 15, 17, 18]. Zhao et al. [18] reported that they obtained well-dispersed PTFE nanofibrils with a diameter of below 500 nm. This was with a screw speed of 200 rpm and a compounding temperature of 200  $^{\circ}\text{C}$ . Jurczuk et al. [17] obtained PTFE nanofibers with a diameter range of 200 ~ 500 nm (100 rpm and 195  $^{\circ}\text{C}$ ). It is well-known that PTFE particles can easily deform into fibrils under low shear force during processing. Generally, it is not only the strong shear stress [24, 25], but also the high efficiency of the stress transfer [25] that forms the fine PTFE fibrils. The shear stress could be stronger with an elevated screw speed, and it could be more effectively transferred



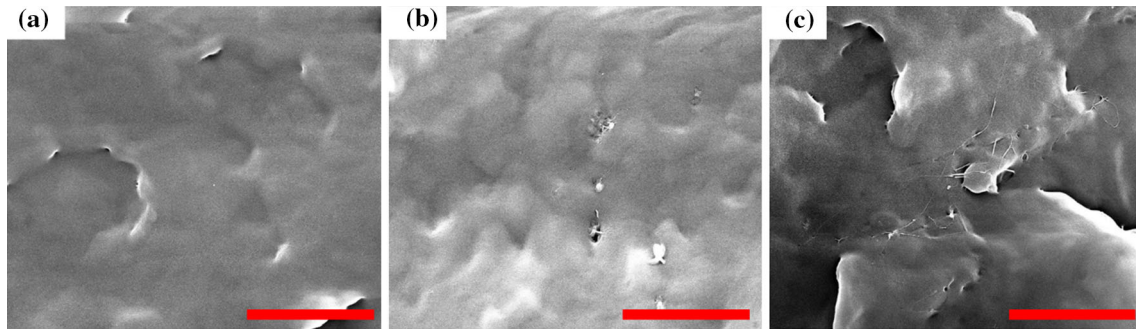
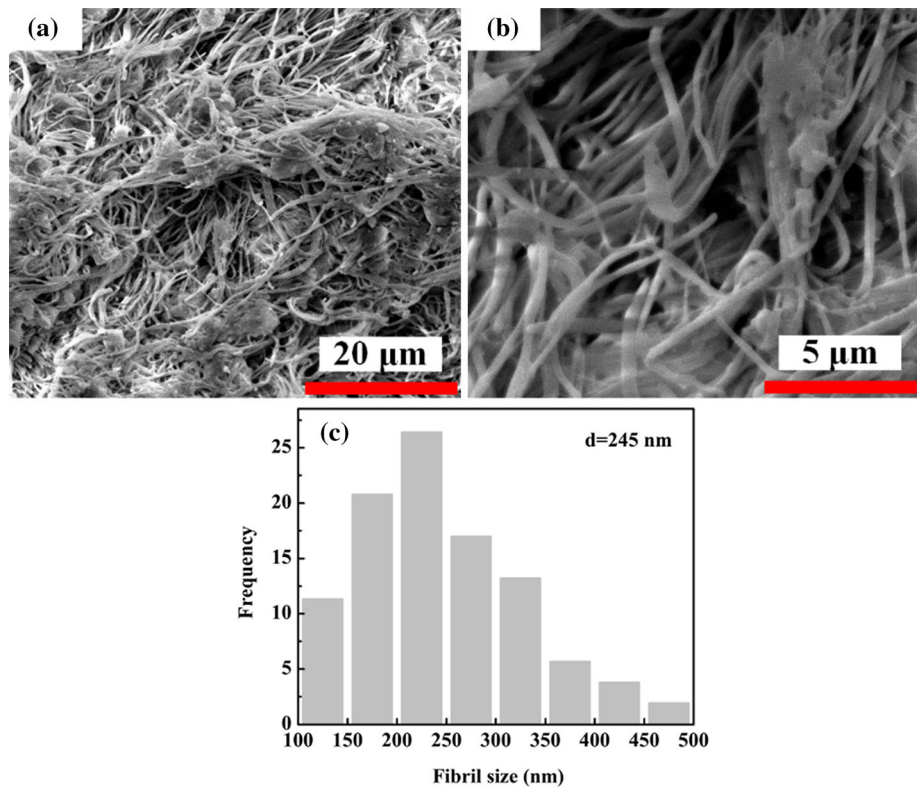


**Figure 1** SEM images of the fractured surface for PP/PTFE blends: **a** neat PP, **b** PP/PTFE (99/1) and **c** PP/PTFE (97/3). The scale bar is 5  $\mu\text{m}$ .

**Figure 2** SEM micrographs of PTFE nanofiber in PP/PTFE (97/3) composites after removing PP: **a** low magnification, **b** high magnification and **c** distribution of the PTFE fiber size.



from the matrix to the PTFE particles at a lower temperature. In this study, the PTFE fibrils with a relatively small diameter were generated due to both the lower process temperature (190 °C) and the higher screw speed (250 rpm). However, the presence of the junctions might have resulted from the entanglements of numerous PTFE nanofibrils under the high shear stress. The 3-D network could enhance the melt strength, stabilizing the cellular structure, and improving the foamability.

Analysis of non-isothermal crystallization behavior.

### Measured crystallization temperature, degree of crystallinity and relative crystallinity

Figure 3 depicts the DSC cooling curves of the non-isothermal crystallization for both the neat PP and PP/PTFE nanofibril composites. Clearly, both the onset temperature ( $T_{\text{onset}}$ ) and the peak ( $T_{\text{p}}$ ) temperature of crystallization shifted to lower temperatures with increasing cooling rate. Under the high cooling rate, a lower time is allowed for polymers to crystallize, which leads to a high undercooling required to initiate the crystallization. While, if the cooling rate

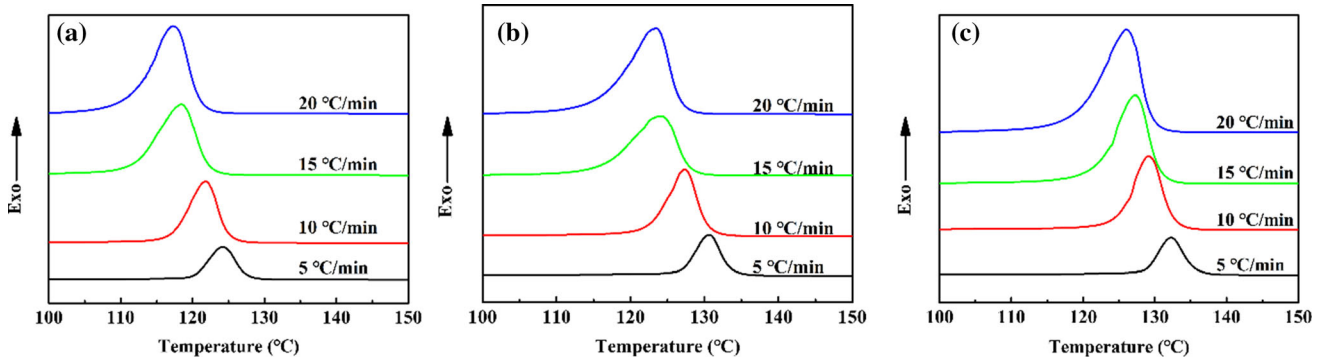


**Figure 3** DSC cooling curves for neat PP and PP/PTFE nanofibril composites at different cooling rates: **a** neat PP, **b** PP/PTFE (99/1) and **c** PP/PTFE (97/3).

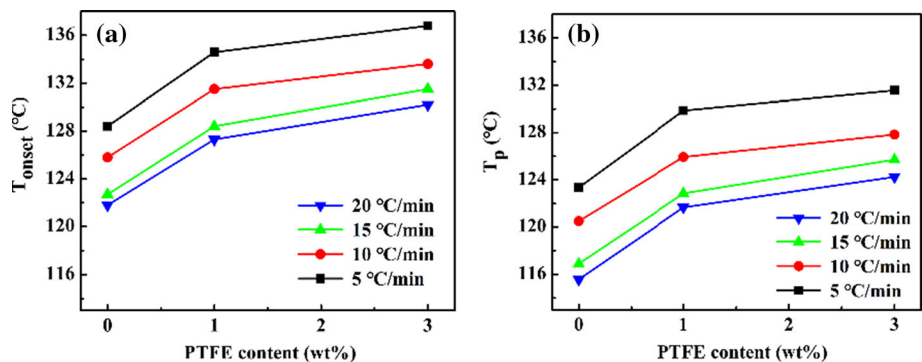
is low, more time should be allowed for polymer molecules to overcome the energy barrier, and thus crystallization will start at higher temperature [30]. Under the same cooling rate, higher  $T_{onset}$  and  $T_p$  were obtained with PTFE fibrils, which can be seen from Fig. 4. This was attributed to the heterogeneous nucleation effect created by PTFE fibers. A similar phenomenon was previously described in Refs.[10, 17, 18, 31].

Figure 5 shows the total crystallinity of neat PP and PP/PTFE composites at the same cooling rate. PP/PTEF (99/1) exhibited crystallinities similar to those of neat PP, whereas PP/PTEF (99/3) exhibited crystallinities lower than those of neat PP, especially at the low cooling rate of 5 °C/min.

The relative crystallinities ( $X_t$ ) as a function of temperature ( $T$ ) and time ( $t$ ) are displayed in Figs. 6 and 7, respectively. The former was calculated following Eq. 1, and the latter was obtained by converting the temperature to time using Eq. 2.

$$X_t = \frac{\int_{T_0}^T \left(\frac{dH_c}{dT}\right) dT}{\int_{T_0}^{T_\infty} \left(\frac{dH_c}{dT}\right) dT} \quad (1)$$

**Figure 4** Non-isothermal crystallization behavior of neat PP and PP/PTFE nanofibril composites: **a** the onset temperature ( $T_{onset}$ ) and **b** the peak ( $T_p$ ) temperature of crystallization as a function of the PTFE content.



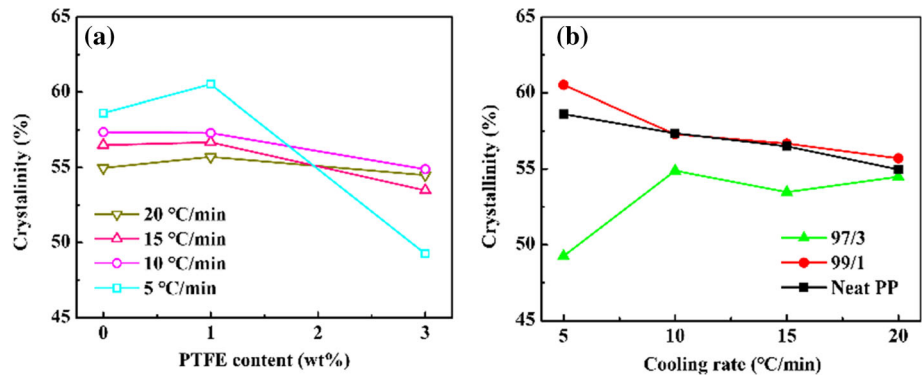
$$t = \frac{|T_0 - T|}{\Phi} \quad (2)$$

where  $T_0$  and  $T_\infty$  are the onset and final temperatures of crystallization, respectively.  $dH_c$  is the enthalpy of the crystallization released during  $dT$ .  $T_t$  represents the temperature at the crystallization time  $t$ , and  $\Phi$  is the cooling rate. Evidently, all the curves exhibited a sigmoidal shape. Under the same cooling rate, the curves shifted to the right side of the temperature axis with the PTFE content, suggesting that crystallization took place at a higher temperature. However, the curve of  $X_t$  as a function of time exhibited a different shift at a varied cooling rate.

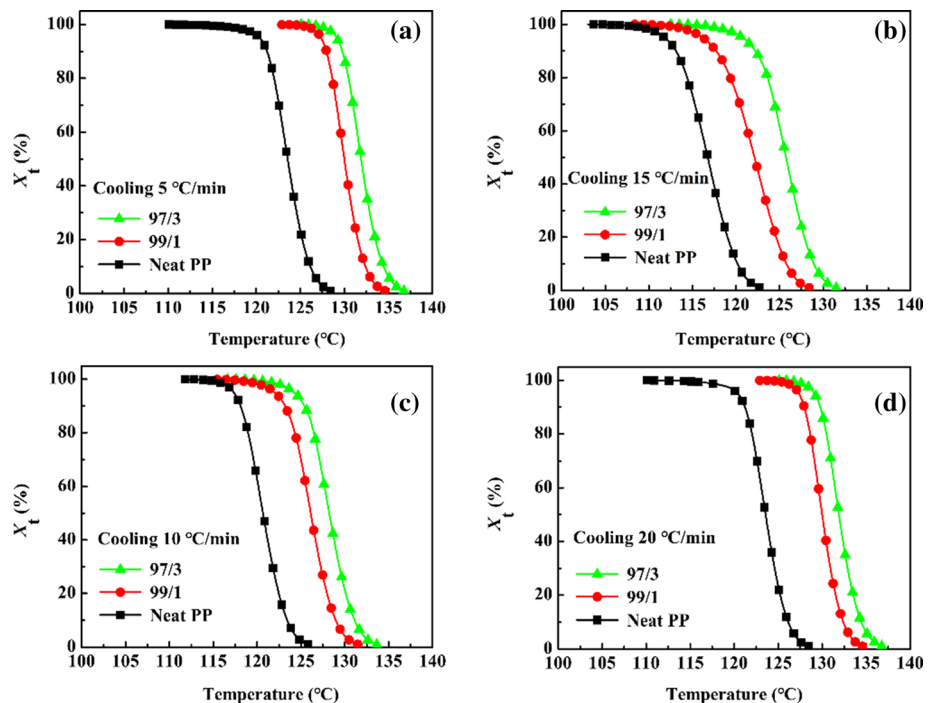
### Analysis of the crystallization kinetics using Avrami, Ozawa, and Mo equations

In order to gain a more detailed insight of the crystallization behavior of PP and its composites, the kinetic analysis of non-isothermal crystallization was carried out with reference to the popular models proposed in the literature, including the modified Avrami [32], Ozawa [33, 34], and Mo equations

**Figure 5** Total crystallinity of neat PP and PP/PTFE composites as a function of **a** PTFE content and **b** cooling rate (for DSC curves of second heating (melting) curve, Figure S2).



**Figure 6** The relationship of  $X_t$  as a function of temperature ( $T$ ) for neat PP and PP/PTFE nanofibril composites at different cooling rates: **a** 5 °C/min, **b** 10 °C/min, **c** 15 °C/min, and **d** 20 °C/min.



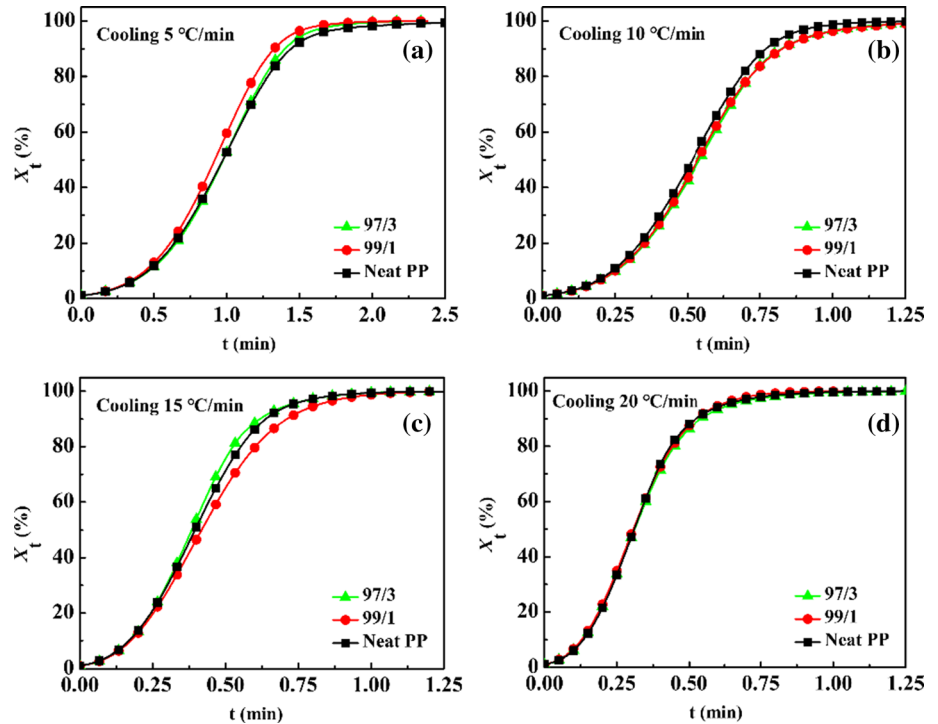
[35, 36]. The Avrami equation [37, 38] (equation S1) is used to analyze the isothermal crystallization. Considering the effect of cooling rate, Jeziorny [32] defines a new crystallization constant  $Z_c$  (equation S3) to describe nonisothermal crystallization.

Figure S3 shows the plots of  $\ln[-\ln(1-X_t)]$  versus  $\ln t$  based on the Avrami model for neat PP and composites at different cooling rates. These plots displayed a linear portion at the initial stage followed by an obvious deviation. This indicated that the modified Avrami model was not applicable in this study. Similar failures of fitting were also demonstrated in other PP composites [30, 39–42]. Such results might be attributed to the temperature changing instantaneously [42] or to the presence of secondary crystallization [43].

Given that the cooling rate  $\Phi$  is an important factor, Ozawa incorporated it in a modified Avrami equation. This is expressed in equation (S4) [33, 34], Figure S4 presents the Ozawa plots of  $\ln[-\ln(1-X_t)]$  versus  $\ln \Phi$ . The plots showed a severe deviation from linearity as  $\Phi$  varied from 5 to 20 °C/min, suggesting that the Ozawa equation was also not appropriate to describe the non-isothermal crystallization of the PP and the PP/PTFE nanofibril composites.

The inability to find adequate descriptions using these two models for non-isothermal crystallization, led to a more reasonable approach for the non-isothermal crystallization of the samples. This approach was proposed by Mo and his co-workers. It is a combination of the Avrami and Ozawa equations and is expressed in Eq. 3 [35, 36], where  $\alpha = n/m$  and

**Figure 7** The relationship of  $X_t$  as a function of time ( $t$ ) for neat PP and PP/PTFE nanofibril composites at different cooling rates: **a** 5 °C/min, **b** 10 °C/min, **c** 15 °C/min and **d** 20 °C/min.



$F(T) = [K(T)/Z_t]^{1/m}$ .  $F(T)$  refers to the cooling rate required to achieve a defined relative crystallinity at a unit of crystallization time.

$$\ln \Phi = \ln(F(T)) - \alpha \ln t \tag{3}$$

Figure 8 displays the fitted plots based on the Mo equation. Straight lines are clearly produced for both the neat PP and the composites, with the regressive coefficient being greater than 0.98. This suggested that the Mo equation successfully described the non-isothermal crystallization process. Table 1 shows the  $\alpha$  and  $F(T)$  values, which were determined from the slopes and intercepts of the fitted lines, respectively. Table 1 also shows that the variation in the value of  $\alpha$

was rather small and was 1.15 – 1.43 for all of the samples, which further validated the Mo equation.

Apparently, the  $F(T)$  value increased with  $X_t$  from 20 to 80% in all cases. The increase in the  $F(T)$  value indicated that a higher cooling rate was required to achieve high crystallinity at the unit time of crystallization. Furthermore, at a given  $X_t$ , the addition of 1% PTFE decreased the  $F(T)$ , which suggested that the crystallization kinetics of the composites containing 1% PTFE was faster than that of neat PP. However, the  $F(T)$  values increased again for the composites containing 3% PTFE. This means the crystallization process was inhibited by the further increase in the PTFE fibril content. Such a phenomenon was closely related to the PTFE network

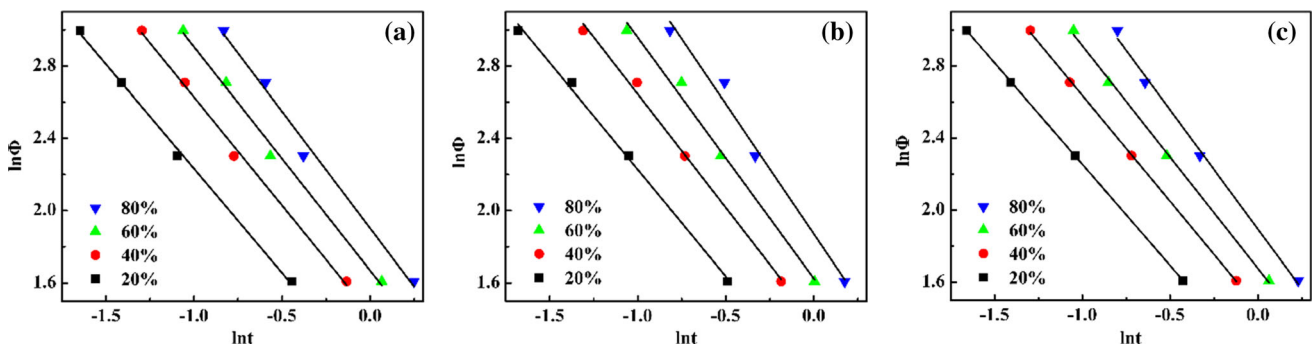


**Figure 8** Fitted plots of samples according to the Mo equation: **a** neat PP, **b** 99/1 and **c** 97/3.



**Table 1**  $F(T)$  and  $\alpha$  of non-isothermal crystallization for samples by the Mo method

Samples	$X_t$ (%)	$F(T)$	$\alpha$
Neat PP	20	2.94	1.15
	40	4.18	1.20
	60	5.31	1.23
	80	6.70	1.29
99/1	20	2.85	1.18
	40	4.01	1.26
	60	5.08	1.33
	80	6.50	1.44
97/3	20	3.10	1.12
	40	4.31	1.18
	60	5.35	1.23
	80	6.65	1.32

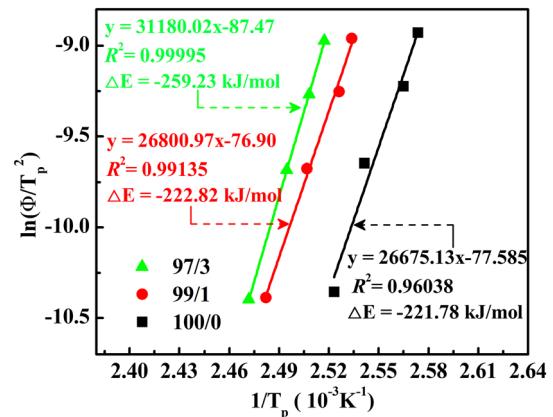
that was simultaneously promoting nucleation by acting as a heterogeneous nucleation agent, and also hindering crystal growth by restraining the polymer chain mobility via the increased crystal–crystal interactions in the PP phase during non-isothermal crystallization. The detailed mechanism will be discussed later in this paper.

### Activation energy of non-isothermal crystallization using Kissinger equation

Given that the cooling rate significantly influences the non-isothermal crystallization process, a theoretical model proposed by Kissinger [44] could be applied to identify the activation energy ( $\Delta E$ , kJ/mol) of non-isothermal crystallization quantitatively, as described in Eq. 4.

$$\frac{d[\ln(\Phi/T_p^2)]}{d(1/T_p)} = \frac{-\Delta(E)}{R} \quad (4)$$

where  $R$  is the gas constant and equals 8.314 J/(k mol),  $T_p$  is the peak crystallization temperature (K). Figure 9 presents the fitted plots of  $\ln(\Phi/T_p^2)$  versus  $1/T_p$  including the fitted equations, the regressive coefficient ( $R^2$ ) and the  $\Delta E$ . The absolute value of  $\Delta E$  for the neat PP was 221.78 kJ/mol. It was raised slightly to 222.82 kJ/mol for the PP/PTFE (99/1), while it increased remarkably to 259.23 kJ/mol in the PP/PTFE (97/3). The increased value of  $|\Delta E|$  could be related to the inhibition effect on the chain motions

**Figure 9** Fitted plots of the activation energy of non-isothermal crystallization for samples based on the Kissinger method.

caused by the existing PTFE nanofibrils. At a low concentration of PTFE (1%), the impeding influence was much weaker, showing a negligible increase in the  $|\Delta E|$  value. However, this restraining mechanism became dominant with a high PTFE content (3%), exhibiting a significantly higher  $|\Delta E|$  value than that of the neat PP.

### Analysis of the crystal nucleation rate

To determine the nucleation effect of the PTFE nanofibrils on PP during non-isothermal crystallization, the nucleation activity was evaluated using Dobreva and Gutzow's methods [45, 46]. The cooling rate ( $\Phi$ ) for homogeneous and heterogeneous nucleation was represented using Eqs. 5 and 6, respectively. Here,  $\Delta T_p$  is given by  $T_m - T_p$  ( $T_m$  is the peak melting temperature).

$$\ln \Phi = A - B/\Delta(T_p^2) \quad (5)$$

$$\ln \Phi = A - B^*/\Delta(T_p^2) \quad (6)$$

where  $A$ ,  $B$ , and  $B^*$  are constants;  $A$  is obtained from the vertical axis intercept of the best fitting lines for the data plotted in Fig. 10.  $B$  and  $B^*$  are obtained from the slopes of the best fitting lines for the neat PP and PP/PTFE nanofibril composites data plotted in Fig. 10, respectively. The nucleation activity ( $\Psi$ ) could be calculated by the ratio of  $B^*$  and  $B$  derived from Eqs. 5 and 6, Queryrespectively; that is,  $\Psi = B^*/B$ . According to the theory, the  $\Psi$  value should be close to 0 if the nucleation activity of a foreign substance (the added disperse phase) is sufficiently high.

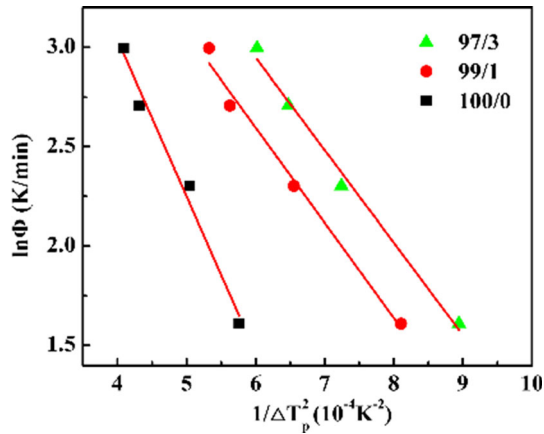


**Figure 10** Plots of  $\ln\Phi$  versus  $1/\Delta T_p^2$  for PP and PP/PTFE nanofibril composites.

**Table 2** Nucleation activity values of the neat PP and PP/PTFE nanofibril composites

Sample	$B^*$	$B$	$\Psi$
Neat PP	–	7885.77	–
99/1	4790.97	–	0.6075
97/3	4656.40	–	0.5904

However,  $\Psi$  will equal 1 in the case of a foreign substance with no nucleation activity. From the fitted plots and the calculated results shown in Fig. 10 and Table 2, the  $\Psi$  values were 0.607 and 0.590 for PP/PTFE (99/1) and PP/PTFE (97/3), respectively. Both values were lower than 1, and this suggested that the PTFE nanofibrils acted as a nucleating agent. The decrease in the  $\Psi$  value with the PTFE content implied that the nucleation effect was strengthened by the presence of more nanofibrils. This result was supported by the higher  $T_{onset}$  and  $T_p$  values of the fibrillated composites compared with those found for the neat PP.

Polymer crystallization is a process involving the rearrangement of chains, and it ranges from a random to an ordered structure. It consists mainly of two steps of nuclei formation and crystal growth. The crystallization rate is affected by both the nucleation and crystal growth rates. The rate of nucleation could be significantly promoted by the heterogeneous nucleation schemes caused by the second phase. At the same time, the existence of the second phase may

produce a negative effect on crystal growth by hindering the movement of the matrix molecules [47–49]. Firstly, the large surface area of the nanofibril second phase increases the resistance of the matrix molecules’ mobility, and thereby, increases the matrix’s viscosity. Moreover, the large number of crystal nuclei caused by the second phase increases the interaction between the crystals and then increases the entanglement of the matrix molecules [47]. Therefore, these crystals themselves, together with the second phase, have inhibited the ability of the polymer chains to move and hindered the crystal growth, which has had a negative influence on crystal growth. Therefore, the polymer’s apparent crystallization rate resulted from the combination of these two factors.

Under non-isothermal crystallization, the added PTFE nanofibrils acted as a nucleating agent, and this produced a remarkably elevated crystallization temperature (Fig. 3) and improved nucleation activity (Table 2) in PP. Such effects were enhanced by the increased amount of nanofibrils. However, the inhibition influence was also taken into account due to the presence of the fibril networks (Fig. 2). These networks restrained the polymer chain motion and increased crystal-crystal interaction, and thus impeded crystal growth during the crystallization process. Such inhibition might have increased the activation energy ( $\Delta E$ ) barrier. In the PP/PTFE (99/1), the low PTFE content and the limited number of crystal nuclei made the inhibition effect relatively weak. The nanofibrils’ positive influence on the crystallization process was dominant. Therefore, the crystallization rate was accelerated accordingly, and it showed decreased  $F(T)$  values, which required a cooling rate for a defined relative crystallinity at the unit time, in contrast to the neat PP. Moreover, the  $\Delta E$  value was slightly increased because the inhibition effect was weak. However, in the case of PP/PTFE (97/3), the larger number of crystal nuclei caused by the larger number of PTFE nanofibrils greatly increased the entanglement of the PP molecules. Moreover, the restriction of a high PTFE content on the movement of the PP molecule should not be neglected. As a result, the fibril networks’ negative influence became overwhelming, and this increased the  $F(T)$  value to even higher than that for the neat PP. Accordingly, the  $\Delta E$  value sharply increased.

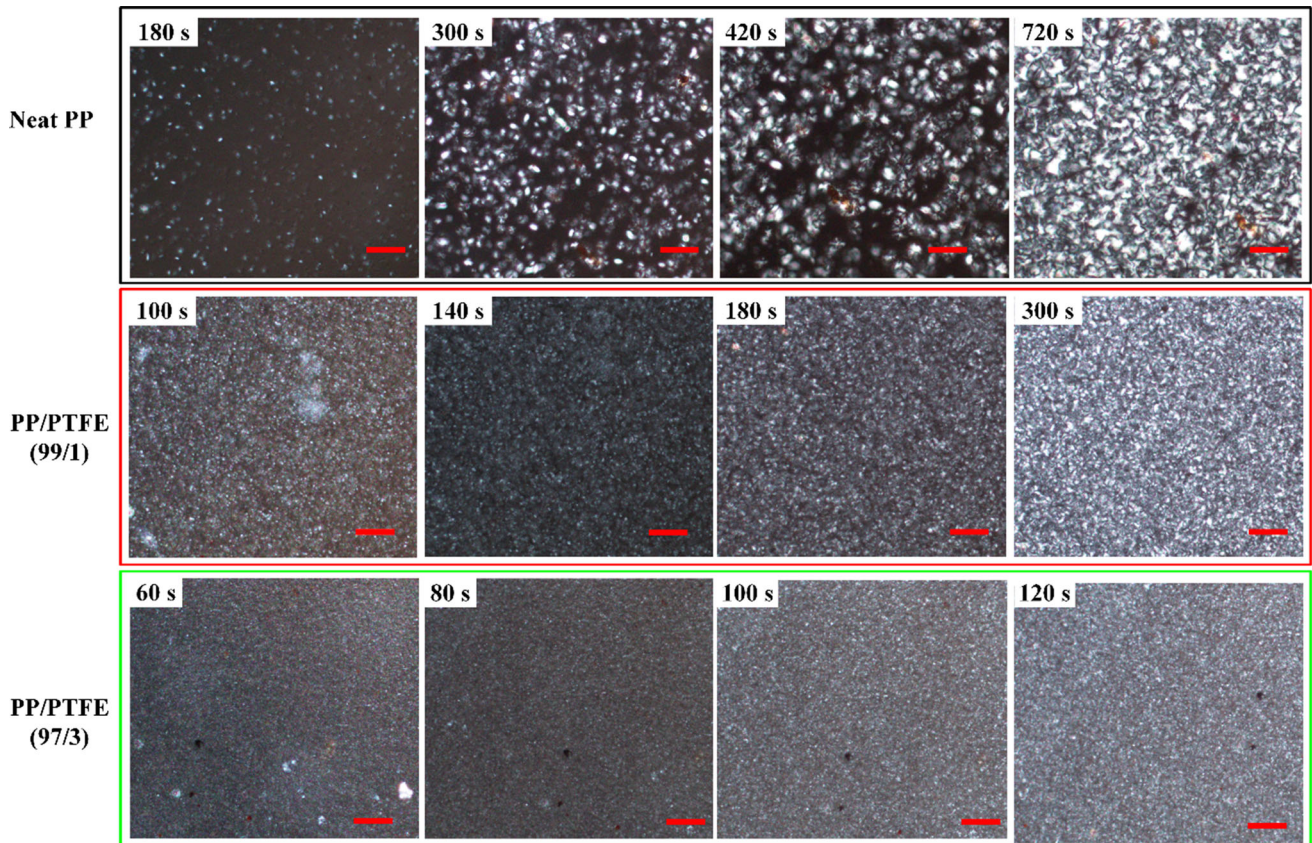


**Figure 11** POM micrographs of neat PP and PP/PTFE composites isothermally crystallized at 140 °C. The scale bar is 50  $\mu\text{m}$ .

### Visualization of PP crystallization with POM

POM micrographs of the isothermally crystallized PP and PP/PTFE-fibril composites are shown in Fig. 11. For PP, it is clear that the crystals existed mainly in the spherulite morphology. A few crystal nuclei appear in the supercooled melt of neat PP within 180 s. By contrast, PP/PTFE composites show more crystal nuclei within 180 s. Moreover, PP/PTFE (97/3) had a higher crystal nuclei density than PP/PTFE (99/1). The existence of a large number of neighboring crystals might generate higher chances of molecular entanglement, thus decreasing the crystal growth rate. Moreover, PTFE fibrils themselves increased the resistance to PP molecule mobility (i.e., increased the viscosity), and thereby decreased the crystal growth rate [50]. Also, the larger the PTFE content, the smaller was the size of PP spherulites. For the neat PP, the time needed for the crystals to fill the view window was 720 s, while for PP/PTFE (99/1) and PP/PTFE (97/3) it was 300 s and 120 s, respectively. This is ascribed to the heterogeneous

nucleation effect of PTFE fibers, which is consistent with the results of nucleation activity. A similar phenomenon has been found for other fibrillated composites [51].

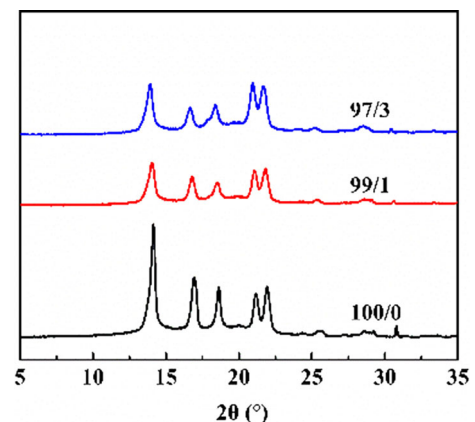


**Figure 12** WAXD profiles of the neat PP and the fibrillated composites.



### Analysis of the crystal structure with WAXD

Figure 12 shows wide angle X-ray diffraction (WAXD) curves of the neat PP and composites after isothermal crystallization at 140 °C (under ambient pressure). Both the PP and PP/PTFE nanofibril composites showed typical  $\alpha$ -crystal reflection signals: (110) at  $2\theta = 14.1^\circ$ , (040) at  $16.9^\circ$ , (130) at  $18.6^\circ$ , (111) + (041) at  $21.1^\circ$ , and (131) at  $21.8^\circ$  [52–54], which means that addition of PTFE does not change the crystal structure of PP under isothermal crystallization.

### Conclusions

In this study, PP/PTFE-fibril composites containing 1 and 3% PTFE were prepared by melt blending. The morphological structure and non-isothermal crystallization behavior of the composites were investigated and compared to those of the neat PP. Kinetic analysis of the crystallization was also conducted.

In the composites, the PTFE had spatial-distribution networks that consisted of fine PTFE nanofibrils with coarse junctions, and these arrangements simultaneously enhanced and inhibited the crystallization process. The crystallization was accelerated for the composites containing 1% PTFE and then depressed for the composites containing 3% PTFE under non-isothermal conditions, which was analyzed using the Mo equation. Due to the combined positive and negative effects caused by the nanofibrils, the activation energy was slightly increased at a low PTFE concentration and was significantly boosted by a high PTFE content. The addition of PTFE led to the appearance of a large number of crystal nuclei. Moreover, the existence of a large number of crystals, together with PTFE itself, might suppress crystal growth by hindering the molecular mobility and by increasing molecular entanglement. For PP/PTFE (99/3), the highest absolute value of  $\Delta E$  corresponds to the highest nucleating activity. Finally, PP and PP/PTFE nanofibril composites showed the same crystal structure.

### Acknowledgements

The authors are also grateful for the China Scholarship Council (201607040007), the donations of PP and

PTFE received from the Braskem Co. Ltd. (U.S.A.) and from the Mitsubishi Rayon Company (Japan), respectively.

### Funding

This work was funded by the National Natural Science fund of China (grant number U1909219), Scientific and Technological Research Project of Henan Province (grand number 202102210028), 111 Project of Henan Province and the National Natural Science fund of China (grant number 51775001).

### Compliance with ethical standards

**Conflicts of interest** The authors declare no conflict of interest.

**Electronic supplementary material:** The online version of this article (<https://doi.org/10.1007/s10853-020-05328-5>) contains supplementary material, which is available to authorized users.

### References

- [1] Leaversuch RD (1996) Enhanced PP resins offer a wide balance of properties Modern plastics USA 26(7):46–49
- [2] Naguib HE, Park CB, Reichelt N (2004) Fundamental foaming mechanisms governing the volume expansion of extruded polypropylene foams. J Appl Polym Sci 91:2661–2668
- [3] Bao J-B, Junior AN, Weng G-S, Wang J, Fang Y-W, Hu G-H (2016) Tensile and impact properties of microcellular isotactic polypropylene (PP) foams obtained by supercritical carbon dioxide. J Supercrits Fluids 111:63–73
- [4] Fu D, Chen F, Kuang T, Li D, Peng X, Chiu DY, Lin CS, Lee LJ (2016) Supercritical CO<sub>2</sub> foaming of pressure-induced-flow processed linear polypropylene. Mater Des 93:509–513
- [5] Ali MABM, Nobukawa S, Yamaguchi M (2011) Morphology development of polytetrafluoroethylene in a polypropylene melt (IUPAC Technical report). Pure Appl Chem 83:1819–1830
- [6] Jurczuk K, Galeski A, Piorowska E (2013) All-polymer nanocomposites with nanofibrillar inclusions generated in situ during compounding. Polymer 54:4617–4628
- [7] Rizvi A, Tabatabaei A, Barzegari MR, Mahmood SH, Park CB (2013) In situ fibrillation of CO<sub>2</sub>-philic polymers: sustainable route to polymer foams in a continuous process. Polymer 54:4645–4652



- [8] Wang K, Wu F, Zhai W, Zheng W (2013) Effect of polytetrafluoroethylene on the foaming behaviors of linear polypropylene in continuous extrusion. *J Appl Polym Sci* 129:2253–2260
- [9] Jurczuk K, Galeski A, Piorkowska E (2014) Strain hardening of molten thermoplastic polymers reinforced with poly (tetrafluoroethylene) nanofibers. *J Rheol* 58:589–605
- [10] Miyamoto R, Utano T, Yasuhara S, Ishihara S, Ohshima M (2015) Effect of crystals and fibrous network polymer additives on cellular morphology of microcellular foams, In AIP Conference proceedings, 040001
- [11] Jurczuk K, Galeski A (2016) Thermoplastic elastomers reinforced with poly (tetrafluoroethylene) nanofibers. *Eur Polym J* 80:58–69
- [12] Peng X-F, Li K-C, Mi H-Y, Jing X, Chen B-Y (2016) Excellent properties and extrusion foaming behavior of PPC/PS/PTFE composites with an in situ fibrillated PTFE nanofibrillar network. *RSC Adv* 6:3176–3185
- [13] van der Meer DW, Milazzo D, Sanguineti A, Vancso GJ (2005) Oriented crystallization and mechanical properties of polypropylene nucleated on fibrillated polytetrafluoroethylene scaffolds. *Polym Eng Sci* 45:458–468
- [14] Yamaguchi M, Yokohara T, Ali MABM (2013) Effect of flexible fibers on rheological properties of poly (lactic acid) composites under elongational flow. *Nihon Reoroji Gakkaishi* 41:129–135
- [15] Ali M, Bin MA, Okamoto K, Yamaguchi M, Kasai T, Koshirai A (2009) Rheological properties for polypropylene modified by polytetrafluoroethylene. *J Polym Sci, Part B: Polym Phys* 47:2008–2014
- [16] Rizvi A (2015) Functional polymer foams from in-situ fibrillated polymer blends University of Toronto
- [17] Jurczuk K, Galeski A, Morawiec J (2017) Effect of poly (tetrafluoroethylene) nanofibers on foaming behavior of linear and branched polypropylenes. *Eur Polym J* 88:171–182
- [18] Zhao J, Zhao Q, Wang C, Guo B, Park CB, Wang G (2017) High thermal insulation and compressive strength polypropylene foams fabricated by high-pressure foam injection molding and mold opening of nano-fibrillar composites. *Mater Des* 131:1–11
- [19] Taki K, Kitano D, Ohshima M (2011) Effect of growing crystalline phase on bubble nucleation in poly (L-lactide)/CO<sub>2</sub> batch foaming. *Ind Eng Chem Res* 50:3247–3252
- [20] Wong A, Guo Y, Park CB (2013) Fundamental mechanisms of cell nucleation in polypropylene foaming with supercritical carbon dioxide—effects of extensional stresses and crystals. *J Supercrit Fluids* 79:142–151
- [21] Nofar M, Guo Y, Park CB (2013) Double crystal melting peak generation for expanded polypropylene bead foam manufacturing. *Ind Eng Chem Res* 52:2297–2303
- [22] Wittmann JC, Smith P (1991) Highly oriented thin films of poly (tetrafluoroethylene) as a substrate for oriented growth of materials. *Nature* 352:414–417
- [23] Yan S, Katzenberg F, Petermann J, Yang D, Shen Y, Straupe C, Wittmann J, Lotz B (2000) A novel epitaxy of isotactic polypropylene ( $\alpha$  phase) on PTFE and organic substrates. *Polymer* 41:2613–2625
- [24] Frey H, Sheiko S, Möller M, Wittmann JC, Lot B (1993) Highly oriented poly (di-n-alkylsilylene) films on oriented PTFE substrates. *Adv Mater* 5:917–919
- [25] Wang C, Hwang L (1996) Transcrystallization of PTFE fiber/PP composites (I) crystallization kinetics and morphology. *J Polym Sci Part B Polym Phys* 34:47–56
- [26] Wang C, Hwang L (1996) Transcrystallization of PTFE fiber/PP composites II effect of transcrystallinity on the interfacial strength. *J Polym Sci Part B Polym Phys* 34:1435–1442
- [27] Sowinski P, Piorkowska E, Boyer SAE, Haudin JM (2016) Nucleation of crystallization of isotactic polypropylene in the gamma form under high pressure in nonisothermal conditions. *Eur Polym J* 85:564–574
- [28] Kuang T, Li K, Chen B, Peng X (2017) Poly (propylene carbonate)-based in situ nanofibrillar biocomposites with enhanced miscibility, dynamic mechanical properties, rheological behavior and extrusion foaming ability. *Compos B Eng* 123:112–123
- [29] Zhao J, Zhao Q, Wang L, Wang C, Guo B, Park CB, Wang G (2018) Development of high thermal insulation and compressive strength BPP foams using mold-opening foam injection molding with in-situ fibrillated PTFE fibers. *Eur Polym J* 98:1–10
- [30] Yuan Q, Awate S, Misra R (2006) Nonisothermal crystallization behavior of polypropylene–clay nanocomposites. *Eur Polym J* 42:1994–2003
- [31] Bernland K, Smith P (2009) Nucleating polymer crystallization with poly (tetrafluoroethylene) nanofibrils. *J Appl Polym Sci* 114:281–287
- [32] Jeziorny A (1978) Parameters characterizing the kinetics of the non-isothermal crystallization of poly(ethylene terephthalate) determined by D.S.C. *Polymer* 19:1142–1144
- [33] Ozawa T (1970) Kinetic analysis of derivative curves in thermal analysis. *J Therm Anal* 2:301–324
- [34] Ozawa T (1971) Kinetics of non-isothermal crystallization. *Polymer* 12:150–158
- [35] Liu T, Mo Z, Wang S, Zhang H (1997) Nonisothermal melt and cold crystallization kinetics of poly (aryl ether ether ketone ketone). *Polym Eng Sci* 37:568–575

- [36] Liu T, Mo Z, Zhang H (1998) Nonisothermal crystallization behavior of a novel poly (aryl ether ketone) PEDEKMK. *J Appl Polym Sci* 67:815–821
- [37] Avrami M (1939) Kinetics of phase change. I General theory. *J Chem Phys* 7:1103–1112
- [38] Avrami M (1940) Kinetics of phase change. II transformation-time relations for random distribution of nuclei. *J Chem Phys* 8:212–224
- [39] Fereidoon A, Ahangari MG, Saedodin S (2009) A DSC study on the nonisothermal crystallization kinetics of polypropylene/single-walled carbon nanotube nanocomposite. *Polym Plast Technol Eng* 48:579–586
- [40] Wu D, Sun Y, Wu L, Zhang M (2008) Linear viscoelastic properties and crystallization behavior of multi-walled carbon nanotube/polypropylene composites. *J Appl Polym Sci* 108:1506–1513
- [41] Huang C-W, Yang T-C, Hung K-C, Xu J-W, Wu J-H (2018) The effect of maleated polypropylene on the non-isothermal crystallization kinetics of wood fiber-reinforced polypropylene composites. *Polymers* 10:382
- [42] Li J, Zhou C, Wang G, Tao Y, Liu Q, Li Y (2002) Isothermal and nonisothermal crystallization kinetics of elastomeric polypropylene. *Polym Test* 21:583–589
- [43] Yang ZH, Wu MH, Chen G, Li SJ, Peng PP, Zhang QL (2016) The effect of montmorillonite modification on crystallization behaviour of polypropylene/montmorillonite composites. *Polym Polym Compos* 24:331–340
- [44] Kissinger HE (1956) Variation of peak temperature with heating rate in differential thermal analysis. *J Res Natl Bur Stand* 57:217–221
- [45] Dobрева A, Gutzow I (1993) Activity of substrates in the catalyzed nucleation of glass-forming melts. II Experimental evidence *J Non-Cryst Solids* 162:13–25
- [46] Dobрева A, Gutzow I (1993) Activity of substrates in the catalyzed nucleation of glass-forming melts. I Theory *J Non-Cryst Solids* 162:1–12
- [47] Nofar M, Zhu W, Park C (2012) Effect of dissolved CO<sub>2</sub> on the crystallization behavior of linear and branched PLA. *Polymer* 53:3341–3353
- [48] Nofar M, Tabatabaei A, Ameli A, Park CB (2013) Comparison of melting and crystallization behaviors of polylactide under high-pressure CO<sub>2</sub>, N<sub>2</sub>, and He. *Polymer* 54:6471–6478
- [49] Nofar M, Tabatabaei A, Park CB (2013) Effects of nano-/micro-sized additives on the crystallization behaviors of PLA and PLA/CO<sub>2</sub> mixtures. *Polymer* 54:2382–2391
- [50] Kakroodi AR, Kazemi Y, Ding W, Ameli A, Park CB (2015) Poly (lactic acid)-based in situ microfibrillar composites with enhanced crystallization kinetics, mechanical properties, rheological behavior, and foaming ability. *Biomacromol* 16:3925–3935
- [51] Kakroodi AR, Kazemi Y, Nofar M, Park CB (2017) Tailoring poly (lactic acid) for packaging applications via the production of fully bio-based in situ microfibrillar composite films. *Chem Eng J* 308:772–782
- [52] Liu H, Zhang L, Liu F, Guo C, Zhang J (2012) Morphological Distribution in Micro-Injected Polypropylene Parts in the Presence of  $\beta$ -Nucleating Agent. *J Macromol Sci, Part B* 51:1566–1582
- [53] Somani RH, Yang L, Hsiao BS, Agarwal PK, Fruitwala HA, Tsou AH (2002) Shear-induced precursor structures in isotactic polypropylene melt by in-situ rheo-SAXS and rheo-WAXD studies. *Macromolecules* 35:9096–9104
- [54] Somani RH, Yang L, Hsiao BS, Sun T, Pogodina NV, Lustiger A (2005) Shear-induced molecular orientation and crystallization in isotactic polypropylene: effects of the deformation rate and strain. *Macromolecules* 38:1244–1255

**Publisher's Note** Springer Nature remains neutral with regard to jurisdictional claims in published maps and institutional affiliations.